nature communications

Article

https://doi.org/10.1038/s41467-026-70724-5

Partitioning of Rubisco activase into the pyrenoidal Rubisco condensate is mediated by a functional protein-protein interaction

Received: 21 July 2025

Accepted: 4 March 2026

Published online: 23 March 2026

Check for updates

Jian Boon How[1], Cheng Wei Poh[1], Yi Siang Ng[1], Tobias Wunder[1,2] & Oliver Mueller-Cajar[1]

Most unicellular microalgae achieve robust photosynthetic CO_2-fixation by sequestering their carboxylase in chloroplastic Rubisco condensates (Rubiscondensates) termed pyrenoids. Only a fraction of the stromal proteome partitions to the Rubiscondensate. One critical pyrenoid component is Rubisco activase (Rca). Here we show that *Chlamydomonas reinhardtii* Rca partitions into the minimal two component EPYC1-Rubisco condensate. We identify the N-terminal domain (NTD) of Rca as containing the responsible sticker motifs. Mutagenesis reveals that single amino acid substitutions previously shown to abolish Rca function also eliminate partitioning. Blue fluorescent protein is excluded from EPYC1-Rubisco condensates, but partitions when fused to the Rca NTD. Expression of an NTD-GFP fusion in the *Chlamydomonas* chloroplast is consistent with the in vitro finding. We hypothesize that partitioning of proteins to biomolecular condensates will frequently utilize pre-existing functionally relevant protein-protein interactions. Identification of the sticker motif provides additional avenues to localize synthetic or phylogenetically remote pyrenoid components to the compartment.

Biological carbon dioxide fixation is almost exclusively catalysed by the enzyme Rubisco. The enzyme is relatively slow and additionally catalysers a side-reaction with oxygen[1]. Most Rubiscos also form inhibited complexes with sugar phosphates that are removed by the action of the molecular chaperone Rubisco activase (Rca)[2,3].

The function of Rubisco in aquatic phototrophs is almost always enhanced by biophysical carbon concentrating mechanisms. In most cases, these involve the compartmentalisation of Rubisco in carboxysomes (prokaryotes)[4] or pyrenoids (eukaryotes)[5,6]. This arrangement then permits the organism to concentrate the abundant substrate bicarbonate near Rubisco, followed by a local equilibration of inorganic carbon species by carbonic anhydrase[7]. It has emerged in the past decade that Rubisco concentration in the green alga *Chlamydomonas reinhardtii* is achieved via liquid-liquid phase separation (LLPS), specifically a complex coacervation between the intrinsically disordered multivalent Rubisco linker protein Essential Pyrenoid Component 1 (EPYC1)[8] and the folded hexadecameric enzyme Rubisco[9,10]. The pyrenoid is known to contain approximately 100 proteins[11,12]. At the same time, the majority of the chloroplast stromal proteins are excluded[13]. For the pyrenoid it has been suggested that Rubisco and EPYC1 form a mesh that excludes components greater than ~80 kDa[12]. More generally, the partitioning and exclusion of client molecules from biomolecular condensates is a critical question of current interest in the field of biomolecular condensates[14].

In this work, we address the partitioning of Rca. This molecular chaperone has been shown to localise to the pyrenoid in vivo[15], and is required to maintain Rubisco function as it continuously removes tightly bound inhibitors from its active sites[3,16]. Meyer et al.[17] earlier identified a Rubisco binding sequence motif present on multiple pyrenoid proteins, predominantly on their C-terminus. For these clients, partitioning is thus determined by binding to the central Rubisco

[1]School of Biological Sciences, Nanyang Technological University, Singapore, Singapore. [2]Present address: Biozentrum der Ludwig-Maximilians-Universität München, Department Biologie I- Botanik, Martinsried, Germany. e-mail: cajar@ntu.edu.sg

organiser. The motif is not found on Rca, suggesting its pyrenoidal localisation is encoded differently.

Some years ago, we demonstrated that Rubisco and EPYC1 are necessary and sufficient to bring about the formation of a dense phase we hypothesised to resemble the *Chlamydomonas* pyrenoid[18]. Here, we extend this work by characterising three-component condensates that include Rca. By interacting with both EPYC1 and Rubisco, Rca readily and specifically partitions to the binary Rubiscondensate, changing its material properties. This localisation is highly fragile as it can be ablated by single amino acid substitutions to the functionally important Rca N-terminal domain. More generally, we propose that utilisation of pre-existing interaction motifs or stickers may be a general feature driving the partitioning of functional condensate components in biology.

Results

Rca partitions into Rubisco-EPYC1 condensates

Coacervation of Rubisco with EPYC1 generates protein-dense droplets that we use as in vitro facsimiles of the pyrenoid. The molecular chaperone Rca is a major component of the pyrenoid and is required to maintain Rubisco in a catalytically competent state. We therefore asked whether the minimal EPYC1-Rubisco droplets were sufficient to partition Rca. *Chlamydomonas reinhardtii* Rca (CrRca) was produced in *Escherichia coli*, and purified to homogeneity. To carboxylate ribulose 1,5-bisphosphate (RuBP), Rubisco needs to be carbamylated at an active site lysine, which then binds a second cofactor Mg^{2+} to form the functional holoenzyme Enzyme-CO_2-Mg^{2+} (ECM). If the apo-enzyme binds the substrate, an inhibited complex Enzyme-RuBP (ER) is formed. Rubisco activase activity is then assayed by comparing the formation of ECM from ER in a spectrophotometric Rubisco assay in the presence and absence of the activase. CrRca was functional as assessed by both ATPase assay and the ability to remove RuBP from the inhibited *Chlamydomonas* Rubisco (Fig. 1a and Supplementary Fig. 1a, b).

We next recapitulated the findings reported in Wunder et al. [18], by forming the binary EPYC1-Rubisco droplets. Quantification of the dense phase using a combination of fluorescence microscopy and sedimentation analysis indicated a dense phase concentration of ~100 mg/ml Rubisco and 11 mg/ml EPYC1 (Supplementary Fig. 1c–f). Under these conditions, light phase concentrations are negligible as assessed by sedimentation assay (Supplementary Fig. 1d). It is noteworthy that physiological Rubisco concentrations in the pyrenoid have been determined to be even higher (~ 350 mg/ml)[15].

When EPYC1-Rubisco droplets were formed in the presence of fluorescently labelled CrRca, all three proteins localised to the dense phase, as demonstrated by both microscopy and sedimentation assays (Fig. 1b, c and Supplementary Fig. 2a). Thus, Rca localisation to the pyrenoid is governed by the presence of Rca-binding stickers on EPYC1, Rubisco or both.

CrRca partitioning was highly salt sensitive. At 100 mM NaCl, EPYC1-Rubisco droplets formed, but Rca no longer partitioned to the dense phase (Fig. 1d). Accordingly, sedimentation assays confirmed that CrRca was mostly found in the light phase when NaCl concentrations exceeded 75 mM (Fig. 1e). The interactions driving Rca partitioning to the condensate are therefore electrostatic in nature.

If multivalent interactions between EPYC1 and Rca are responsible for partitioning, then the two components should form a binary condensate. Indeed, we found that Rca and EPYC1 alone were also able to form a salt-sensitive condensate (Fig. 1f, g).

The properties of the Rubiscondensate can be modulated by CrRca

As reported for the binary Rubiscondensate, the ternary droplets coalesced and relaxed, indicating a liquid property and thus a relatively short lifetime of relevant intermolecular interactions[14] (Fig. 2a).

We probed the mobility of droplet components using fluorescence recovery after photobleaching (FRAP) under two regimens we call excess EPYC1 (10 μM) and limiting EPYC1 (5 μM). In our earlier work[18] we reported rapid recovery of both EPYC1 and Rubisco. However, this early experiment was performed using fluorescent "foreign" cyanobacterial Rubisco. For the binary system containing cognate Rubisco from the alga *Chlamydomonas* and excess EPYC1, we found EPYC1 recovered 37% of its intensity in 30 s. Rubisco, in contrast, had a very slow recovery rate (10% in one minute) (Fig.2b).

Including Rca in this experiment led to a reduction in mobility for all components, where Rubisco and Rca failed to recover, and EPYC1 regained only 20% of fluorescence in 30 s (Fig. 2c). This effect was less pronounced when EPYC1 was limiting (Supplementary Fig. 2c, d). This indicated that Rca-EPYC1 (as opposed to Rca-Rubisco) interactions were mostly responsible for the observed reduction in mobility.

Our data so far suggested that partitioning of Rca to the EPYC1-Rubisco condensate involves electrostatic interactions between all three components. The combined effect of all possible interactions results in a less dynamic condensate when EPYC1 is in excess, reducing the mobility of all proteins. These emergent properties imply that realistic reconstitutions of the compartment for functional studies will be complicated by the need to carefully titrate multiple assay components, including proteins and ionic contributors.

The specificity of Rca partitioning

Next, we asked whether the ability of CrRca to partition to the Rubiscondensate was specific to this protein or whether other negatively charged AAA + ATPases would also readily enter the dense phase. We therefore tested a panel of diverse purified Rubisco activases for this property (Supplementary Fig. 3a). For a long time it has been recognised that for green-type Rcas (found in plants and green algae), there is a functional incompatibility between enzymes derived from Solanaceae and non-Solanaceae species[19,20]. This is determined by the interaction between specificity helix 9 of Rca and the ßC-ßD loop of the Rubisco large subunit[21]. Using *Chlamydomonas* Rubisco, we found this green algal enzyme could be activated by all tested plant activases, but the Solenaceae Rca from tobacco was least functional (Fig. 3a). Strikingly sedimentation assays indicated that the tobacco (Solenaceae)-Rca was mostly excluded from the EPYC1-Rubisco dense phase (Fig. 3b). In contrast all non-Solanaceae Rcas tested (from rice, *Arabidopsis thaliana* and *Agave tequilana*) were found in the EPYC1-Rubisco pellet (Fig. 3b). The unrelated bacterial Rubisco activases RsCbbX[22], AfQ2O2[23] and HnQO)[24] were also largely excluded from EPYC1-Rubisco condensates (Fig. 3b). Equivalent condensates were inspected by microscopy using DyLight 405-labelled activases (Fig. 3c). The distribution of fluorescence was generally consistent with the sedimentation assays with the exception of RsCbbX. This bacterial activase concentrated in clusters within the droplets, which resembled cavities under DIC. In addition, irregular droplet morphologies were observed in multiple cases, as earlier seen in EPYC1 droplets formed by non-cognate Rubiscos[18].

These findings raised the possibility that recruitment of the green-type Rca proteins to the three-component condensate was related to their Rubisco-activating function, specifically their relative ability to productively bind the enzyme.

Partitioning of Rca into the dense phase could theoretically be mediated by interactions with Rubisco, EPYC1 or both. We therefore assessed the ability of different Rca proteins to form condensates with EPYC1 alone. The propensity to phase separate with EPYC1 was shared by most Rca proteins, with the exception of the tobacco Rca (Fig. 3d–f and Supplementary Fig. 3b). Even the bacterial Rca proteins condensed with EPYC1 (Fig. 3b–f).

In summary, EPYC1 displayed a relative promiscuity in its ability to interact and phase separate with different Rca proteins. However, when Rubisco was included in the system, most non-cognate Rca proteins exhibit reduced partitioning to the dense phase (Fig. 3b, c). The ability of Rubisco to outcompete non-specific Rca proteins may imply that EPYC1 utilises identical or overlapping stickers to interact

https://doi.org/10.1038/s41467-026-70724-5

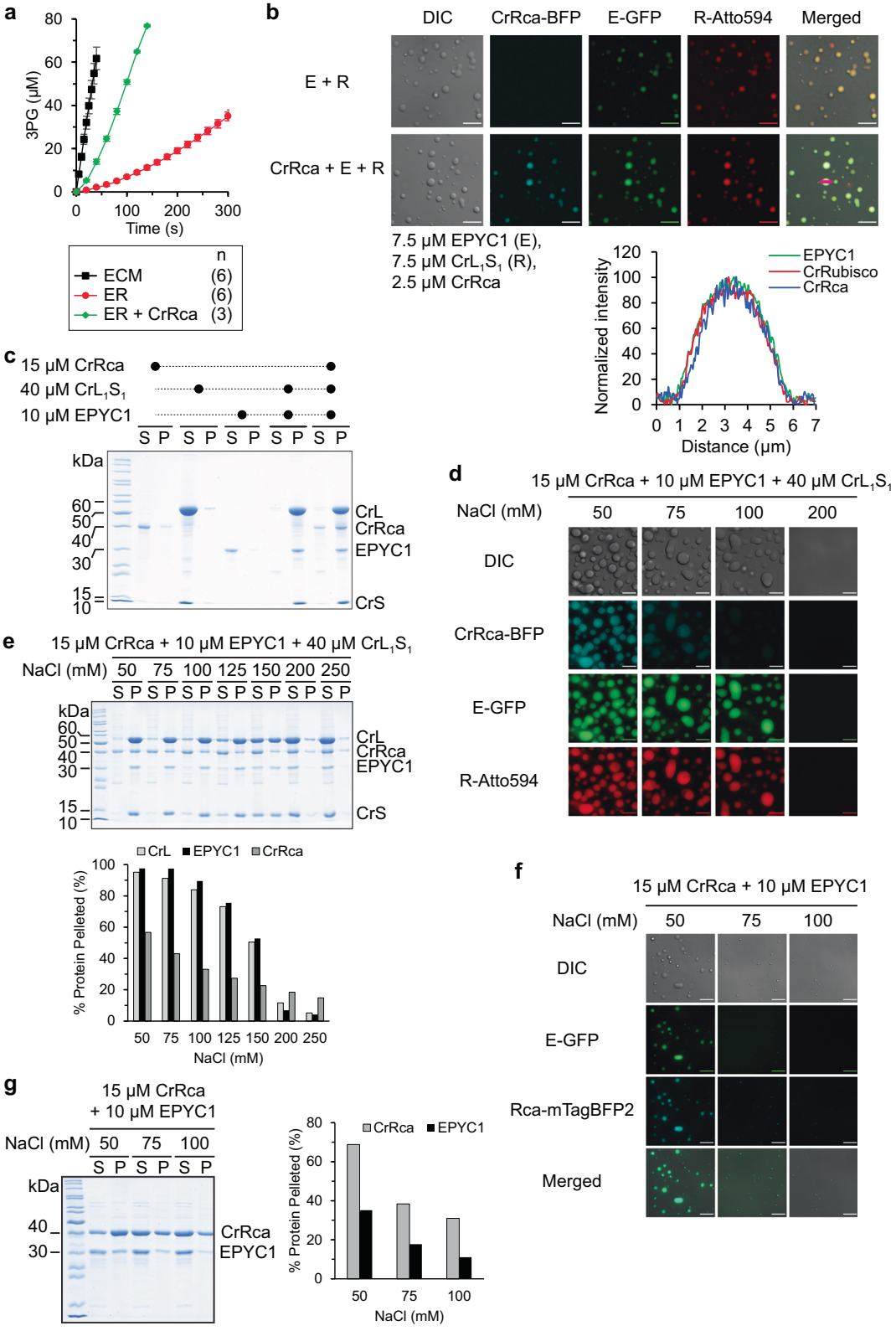

with both Rca and Rubisco. Alternatively, the Rubisco-EPYC1 network may sterically exclude the weakly binding, non-specific Rca proteins.

The Rca N-domain is essential for partitioning into the EPYC1-Rubisco condensates

Green-type Rcas possess an intrinsically disordered N-terminal domain (residues 1–61), which is essential for Rca function (Fig. 4a and Supplementary Fig. 4). The importance of this domain has been appreciated for decades, as demonstrated by both single amino acid substitutions and truncations[25–28]. We produced and purified a truncated CrRca lacking residues 1-61 and multiple point mutants of the conserved Trp-9 and Ser-19 residues (Supplementary Fig. 5a). Ser-19 has been reported to be phosphorylated[29,30], and in plants, the analogous phosphorylation is thought to inactivate the enzyme in the

Fig. 1 | Rubisco activase (CrRca) partitions to the binary Rubisco-EPYC1 condensate. a Purified CrRca is functional. The spectrophotometric Rubisco activase assay was conducted using 0.2 μM Rubisco and 5 μM CrRca. Technical replicates were performed for ECM, ER ($n = 6$) and ER + CrRca ($n = 3$). Error bars indicate the mean and s.d. of 3PG produced. ECM-activated Rubisco (Enzyme-CO_2-Mg^{2+}), ER-inhibited Rubisco (Enzyme-RuBP). **b** Representative micrographs of CrRca recruitment into EPYC1-CrRubisco condensates. The pink line denotes a single droplet whose fluorescence intensity plot was depicted. Proportions of labelled components: 1.33% EPYC1-GFP, 2.67% Atto 594-labelled CrRubisco, 22% CrRca-BFP. Protein concentrations refer to monomers/ active sites for Rubisco (CrL_1S_1). Representative data of 2 independent experiments are shown ($n = 2$). **c** The majority of CrRca partitions into the condensates as assessed via droplet sedimentation assays. S, supernatant; P, pellet. Representative data of 3 independent experiments are shown ($n = 3$). **d**, **e** CrRca partitioning is salt sensitive as shown using microscopy (**d**) and sedimentation assay (**e**). The experiments were performed once ($n = 1$). **f**, **g** CrRca can condense with EPYC1 alone at low salt concentrations as shown using microscopy (**f**, spiked with 3% EPYC1-GFP and 1% CrRca-BFP, experiment performed once ($n = 1$)) and sedimentation assay. Representative data of 2 independent experiments are shown ($n = 2$). **g** Scale bars: 10 μm. Source data are provided as a Source Data file.

dark[31,32]. The variant proteins possessed similar ATPase activity rates as the wild-type. As expected, the ability to activate Rubisco was abolished (Fig. 4b). Sedimentation and microscopy assays indicated that deletion of the N-terminal 61 residues eliminated both phase separation with EPYC1 and partitioning into EPYC1-Rubisco droplets (Fig. 4c–f). The three-point mutants condensed with EPYC1 (Fig. 4c, e and f), but did not sediment with the dense phase when exposed to EPYC1-Rubisco (Fig. 4d, e).

Therefore, the N-terminal domain of Rca interacts with both EPYC1 and Rubisco. We produced a panel of fluorescent N-domain fusion proteins (CrN61-mTagBFP2, abbreviated as CrN-BFP) harbouring the wild-type N-domain and the three substitutions (Fig. 5a and Supplementary Fig. 6a, b). The wild-type N-domain caused the fusion protein to partition into the condensate, an attribute that was completely abolished by the three-point mutations (Fig. 5a). The microscopy data indicated that these variants were in fact, depleted in the dense phase. The partitioning property of the N-terminal fusion protein was similarly salt sensitive as Rca partitioning (Fig. 5b). Direct binding of CrN-BFP to Rubisco could be detected by a Native-PAGE gel shift assay, where CrN-BFP caused a concentration-dependent retardation in electrophoretic migration (Fig. 5c). In contrast, the CrN-BFP point mutants did not elicit this gel shift (Fig. 5d). Subsequent multiple attempts to visualise the N-terminal domain bound to Rubisco by cryo-electron microscopy have been unsuccessful thus far, possibly due to high heterogeneity in the binding mode.

Finally, we used chloroplast transformation[33] to generate *Chlamydomonas* lines expressing chloroplastic CrN-mVenus and mVenus. This procedure selects for homologous recombination of the expression vector with the plastome to restore photosynthetic function of a *psbH* mutant and results in the isolation of markerless transformants with gene expression driven by the *psaA*-exon1 promoter[33]. mVenus alone localised throughout the chloroplast stroma, but importantly was excluded from the pyrenoid. In contrast, CrN-mVenus resulted in a partial enrichment of the signal in the pyrenoid (Fig. 5e and Supplementary Fig. 7). We also imaged lines generated earlier by the Jonikas group where fluorescently tagged full-length pyrenoid components EPYC1, RbcS and Rca were expressed following transformation of the nuclear genome[8]. For these proteins, partitioning to the pyrenoid appeared to be absolute (Fig. 5e and Supplementary Fig. 7). These findings confirm that the N-terminal domain of Rca is sufficient to convert mVenus into a pyrenoid client in vivo.

Discussion

In contrast to many other biomolecular condensates, the Rubisco-condensates associated with pyrenoids and carboxysomes have a clearly defined physiological function, which completely relies on the concentration of Rubisco active sites close to a source of the gas carbon dioxide[10]. To achieve this goal, it is critical that space is used efficiently and a highly selective compartment is established. Here, we use an in vitro system to dissect the partitioning determinants of Rubisco's chaperone Rca and demonstrate that this property is specific and easily perturbed.

In this phase-separated system we find that Rca forms multivalent and salt-sensitive interactions with both of the two main components of the pyrenoid, EPYC1 and Rubisco. The interaction with Rubisco is dominated by the previously discovered functional N-terminal interaction. This implies that the ancient pre-existing interaction between Rca and Rubisco was co-opted here to ensure correct localisation of the chaperone in the phase-separated compartment that houses its substrate Rubisco. It will be interesting to see whether the recruitment of pre-existing protein-protein interactions will be found to be a frequently encountered feature of partitioning determinants for biomolecular determinants.

The Rca localisation in our system is extremely fragile, and single amino acid substitutions that eliminate Rca function also abolish partitioning. We do not currently understand the precise interaction between the Rca N-terminal domain and Rubisco, but we hypothesise that the mutations reduce binding. The loss of a single hydroxyl group (e.g., in S19A) abolished both Rca function and partitioning, indicating a critical contribution to the interaction likely by hydrogen bond formation. The physiologically relevant phosphomimetic S19D has the same effect, which would be expected to cause exclusion of the activase upon phosphorylation in vivo. It is therefore possible that the lability of Rca partitioning is related to regulation by phosphorylation, where the inactivated phosphorylated Rca[28,34] is excluded from the compartment.

For the *Chlamydomonas* pyrenoid, it has been shown that mutation of a motif frequently found at the C-terminus of pyrenoid localised proteins leads to stromal dispersion of the protein Cre10.g430350[17]. The motif is highly similar to the EPYC1 repeat region that has been structurally validated to bind to the Rubisco small subunit[9].

More generally, the exclusion of components from biomolecular condensates following mutation has been reported for the stress granule. Deletion of a 14-residue sequence from Ataxin-2 excludes the protein from the compartment[35]. Similarly, a V11A substitution in G3BP1 disrupts an interaction with Caprin-1, reducing stress granule assembly[36].

We find that inclusion of Rca in the ternary condensate can lead to enhanced viscosity and reduced component mobilities. The associated change in material properties is anticipated to modify the functionality of droplet components, complicating relevant analyses. The complexity of the pyrenoid and combinatorial size of the associated experimental space will therefore generate challenges. Along this line of thought, it will also be important to initiate experiments utilising more realistic stromal ionic compositions[37]. The detailed ionic composition of the *Chlamydomonas* pyrenoid or chloroplast stroma is not known. Measurements of 64-223 mM K^+ in the algal chloroplast were reported[38]. Values reported for three plant species in a single study ranged from 41–194 mM K^+, 41–72 mM Na^+ and 89–96 mM Cl^-[39]. These cation values are higher than those used in our experiments, however, their thermodynamic activities are expected to be lower in vivo compared to in vitro due to association with proteins, membranes and other cellular constituents[40].

Overall, we posit that our study provides useful information on the identity and nature of protein-protein interactions driving the assembly of ternary Rubisco condensates. However, we recognise that the findings also imply that a significant gap exists between our droplets and the properties of the cellular compartment.

https://doi.org/10.1038/s41467-026-70724-5

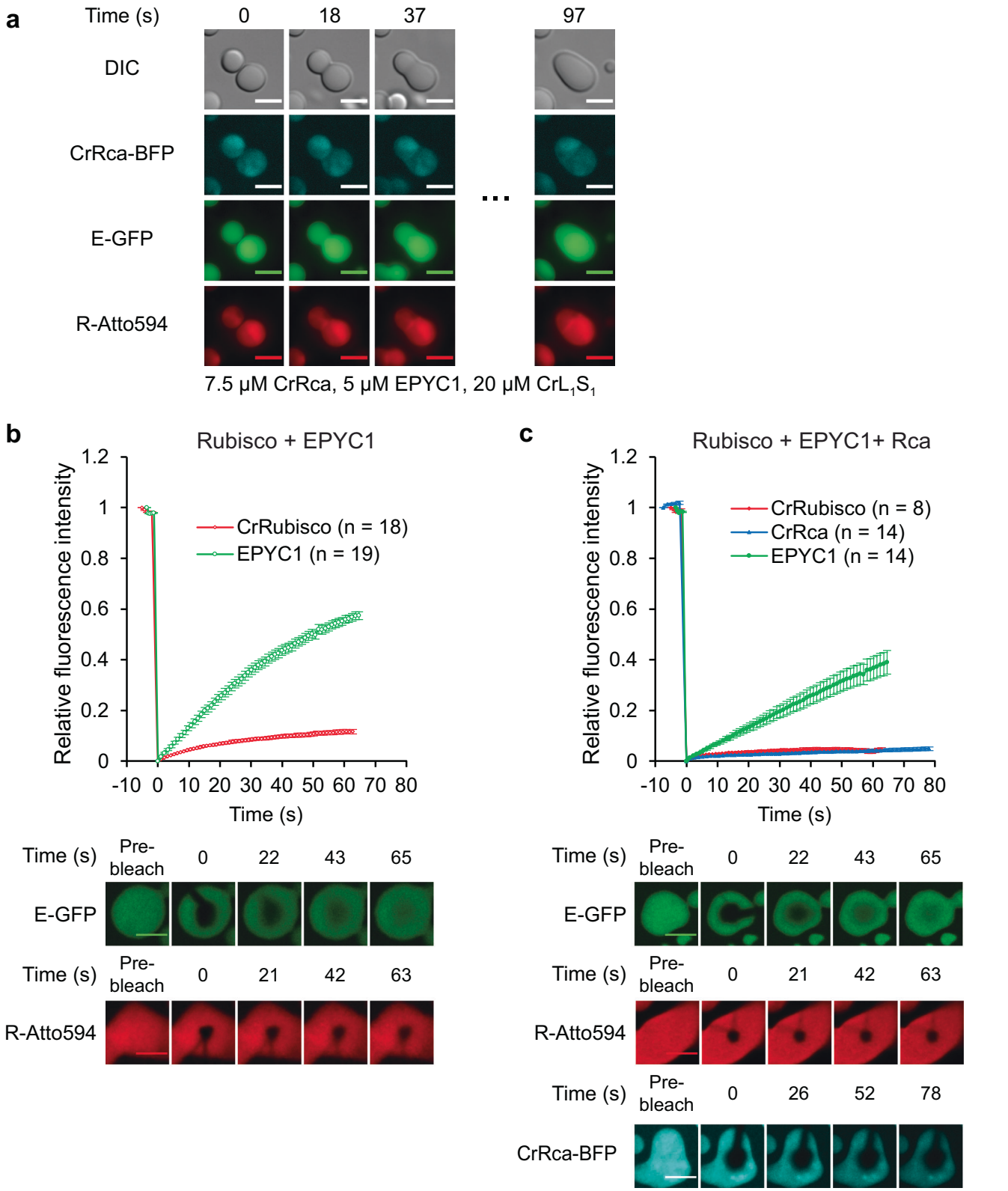

Fig. 2 | Inclusion of Rca alters the material properties of the condensate. a Three component condensates are liquid-like. Proportions of labelled components: 6% EPYC1-GFP, 1% Atto 594-labelled CrRubisco, 4% CrRca-BFP. Scale bars: 5 μm. Representative data of 2 independent experiments are shown ($n = 2$). **b**, **c** FRAP experiments comparing binary (**b**) and ternary (**c**) condensates. Protein concentrations: 10 μM EPYC1, 15 μM Rubisco, 5.6 μM Rca. Scale bar: 5 μm. Fluorophores included are 1.2 μM CrRca-BFP, 0.3 μM EPYC1-GFP and 0.3 μM Atto 594-labelled Rubisco. Bleaching of individual droplets were performed to measure CrRubisco ($n = 18$) and EPYC1 ($n = 19$) for Rubisco + EPYC1 samples and CrRubisco ($n = 8$), CrRca ($n = 14$) and EPYC1 ($n = 14$) for Rubisco + EPYC1 + Rca samples. Error bars indicate mean and SEM of relative fluorescence intensity. Source data are provided as a Source Data file.

https://doi.org/10.1038/s41467-026-70724-5

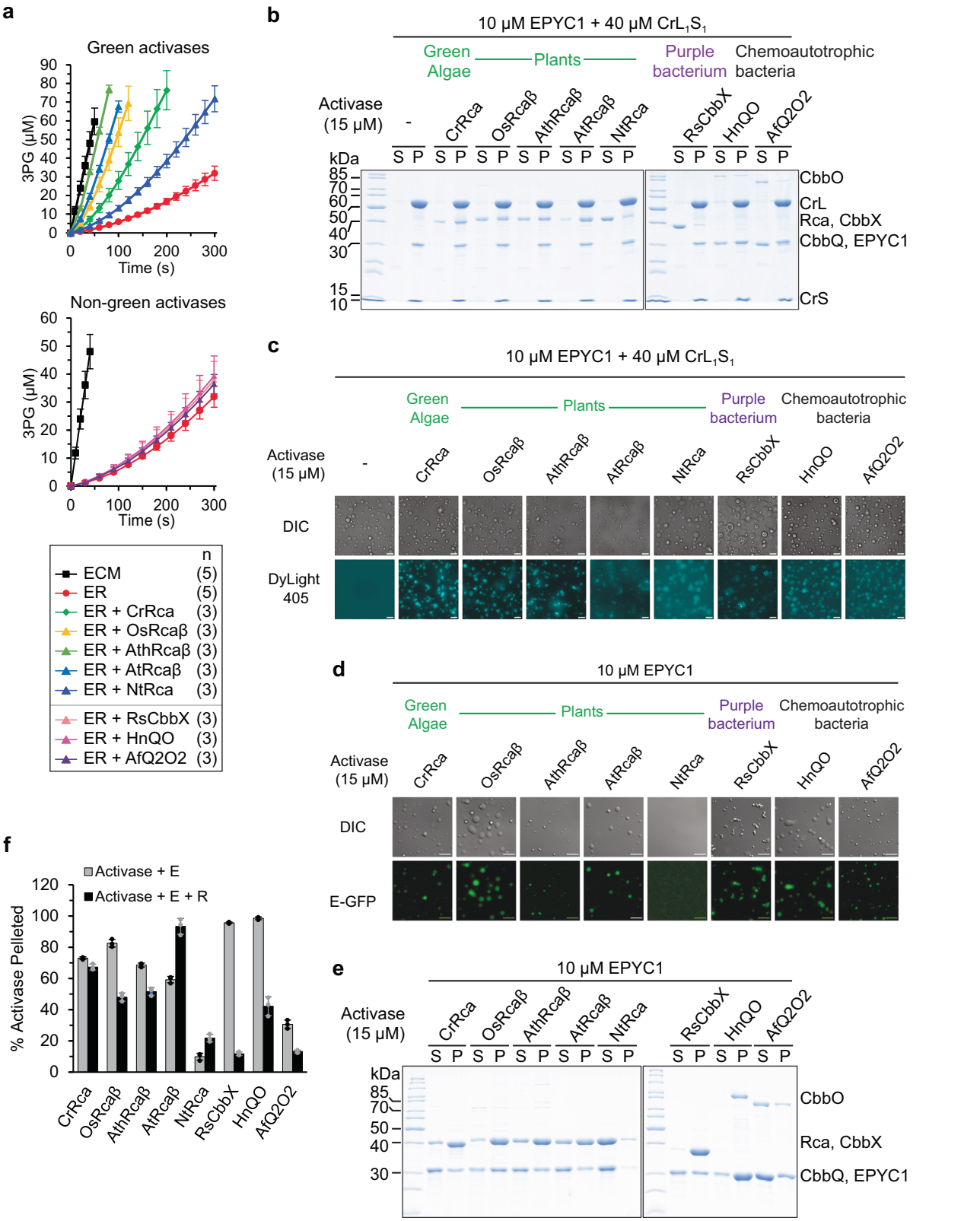

Fig. 3 | The specificity of Rca partitioning. a Spectrophotometric Rubisco activase assays were performed using 0.2 μM Rubisco and 5 μM Rca from different species. Cr, *Chlamydomonas reinhardtii*; Os, *Oryza sativa*; Ath, *Arabidopsis thaliana*; At, *Agave tequilana*; Nt. *Nicotiana tabacum*; Rs, *Rhodobacter sphaeroides*; Hn, *Halothiobacillus neapolitanus*; Af, *Acidithiobacillus ferrooxidans*. n refers to technical replicates. Error bars represent the mean ± S.D. **b** Droplet sedimentation assay indicates functionally compatible green Rca proteins partition to the dense phase. **c** Micrographs of condensates to assess DyLight 405-labelled Rca partitioning. Scale bars: 10 μm. The experiment was performed once ($n = 1$). **d** Multiple Rca proteins can form binary condensates with EPYC1. Reactions contain 0.3 μM EPYC1-GFP. Scale bars: 10 μm. The experiment was performed once ($n = 1$). **e** Sedimentation assays of the reactions shown in (**b**). **f** Densitometric quantification of Rca sedimentation shown in (**b**), (**e**) and their technical replicates ($n = 3$). Error bars indicate the mean and s.d. of the percentage of activase pelleted. Source data are provided as a Source Data file.

https://doi.org/10.1038/s41467-026-70724-5

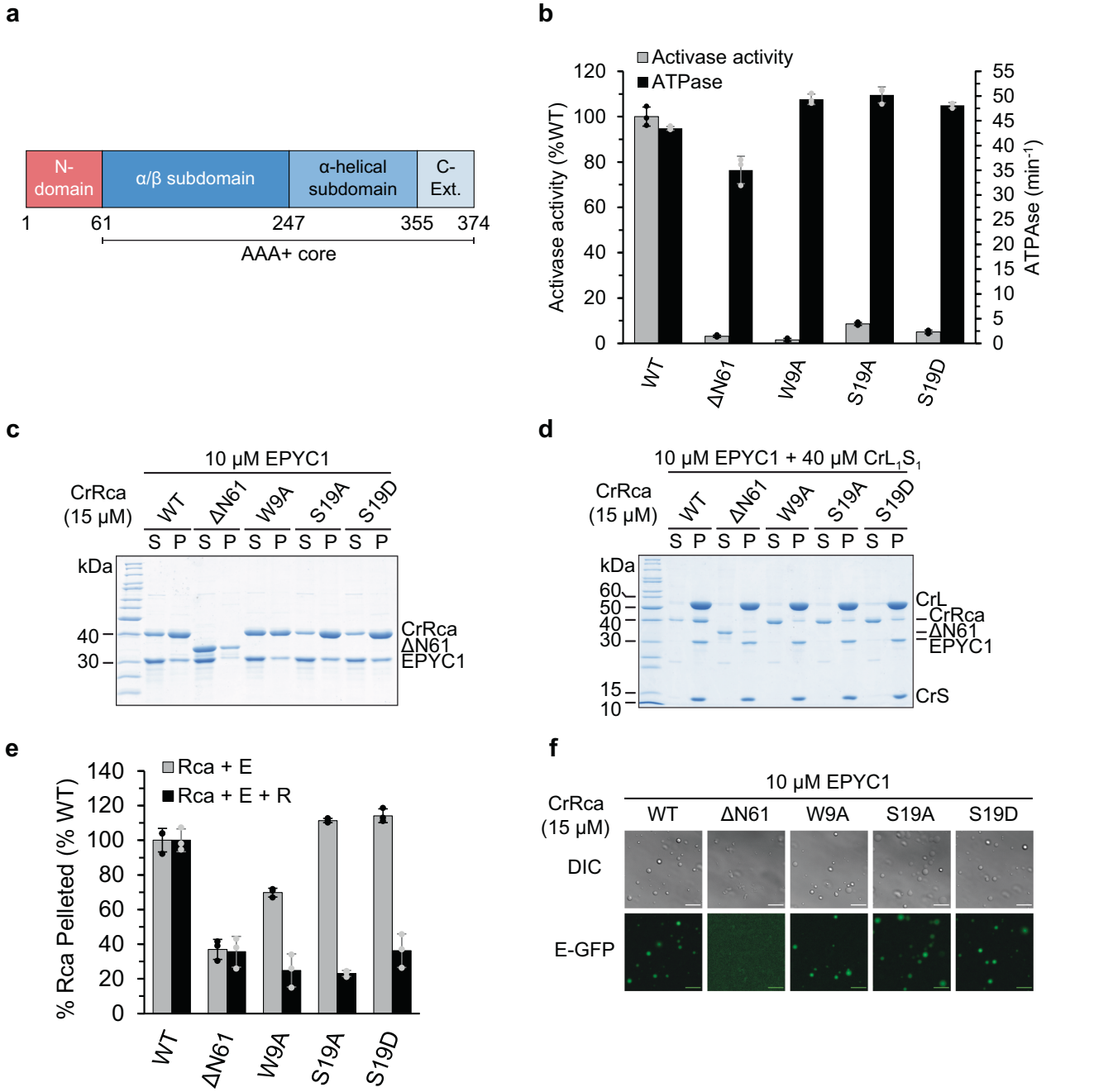

Fig. 4 | Specific N-terminal domain residues dictate Rca partitioning to the Rubiscondensate. a Scheme of Rca indicating the disordered N-terminal domain. **b** N-terminal domain mutants are functional ATPases but are unable to activate Rubisco. Error bars indicate S.D. of three independent experiments ($n = 3$). **c** Sedimentation assay of binary condensates. **d** Sedimentation assay of ternary condensates. The tested variants do not partition to the dense phase. **e** Quantification of sedimentation assays shown in (**c**) and (**d**) comparing binary and ternary condensates. Error bars represent the mean and S.D. from three different experiments ($n = 3$). **f** Micrographs of condensates formed using EPYC1 and the N-terminal domain mutants. Scale bars: 10 μm. Reactions include 0.3 μM EPYC1-GFP. The experiment was performed once ($n = 1$). Source data are provided as a Source Data file.

The interaction of Rca with EPYC1 is less specific than that with Rubisco, and the relevant Rca point mutants are still able to form binary condensates. This property is likely related to the intrinsic disorder of EPYC1, enabling fuzzy binding[41]. However, in the presence of Rubisco, the enzyme outcompeted and excluded those Rca proteins that do not effectively interact with the carboxylase. We consider the interaction between Rca and Rubisco to be site-specific, and the interaction between EPYC1 and Rca to be chemically specific (involving the interaction between two intrinsically disordered proteins)[14]. Both interactions contribute to the final condensate, but the site-specific interaction is clearly dominant.

Our findings suggest that the in vitro pyrenoidal Rubiscondensate is a highly discriminatory compartment, which will not readily accept "contamination" by non-cognate proteins such as BFP. In addition, the stoichiometry of condensate components modulates the properties of the dense phase. It will be fascinating to study whether this specificity extends to the partitioning of small molecules[14] such as the multiple small ions (such as RuBP and ATP) that are critical to Calvin cycle function. In translational projects that aim to transplant the pyrenoid into land plants[42,43] it may be useful to evaluate the basis of partitioning and possibly engineer more robust localisation for critical components.

https://doi.org/10.1038/s41467-026-70724-5

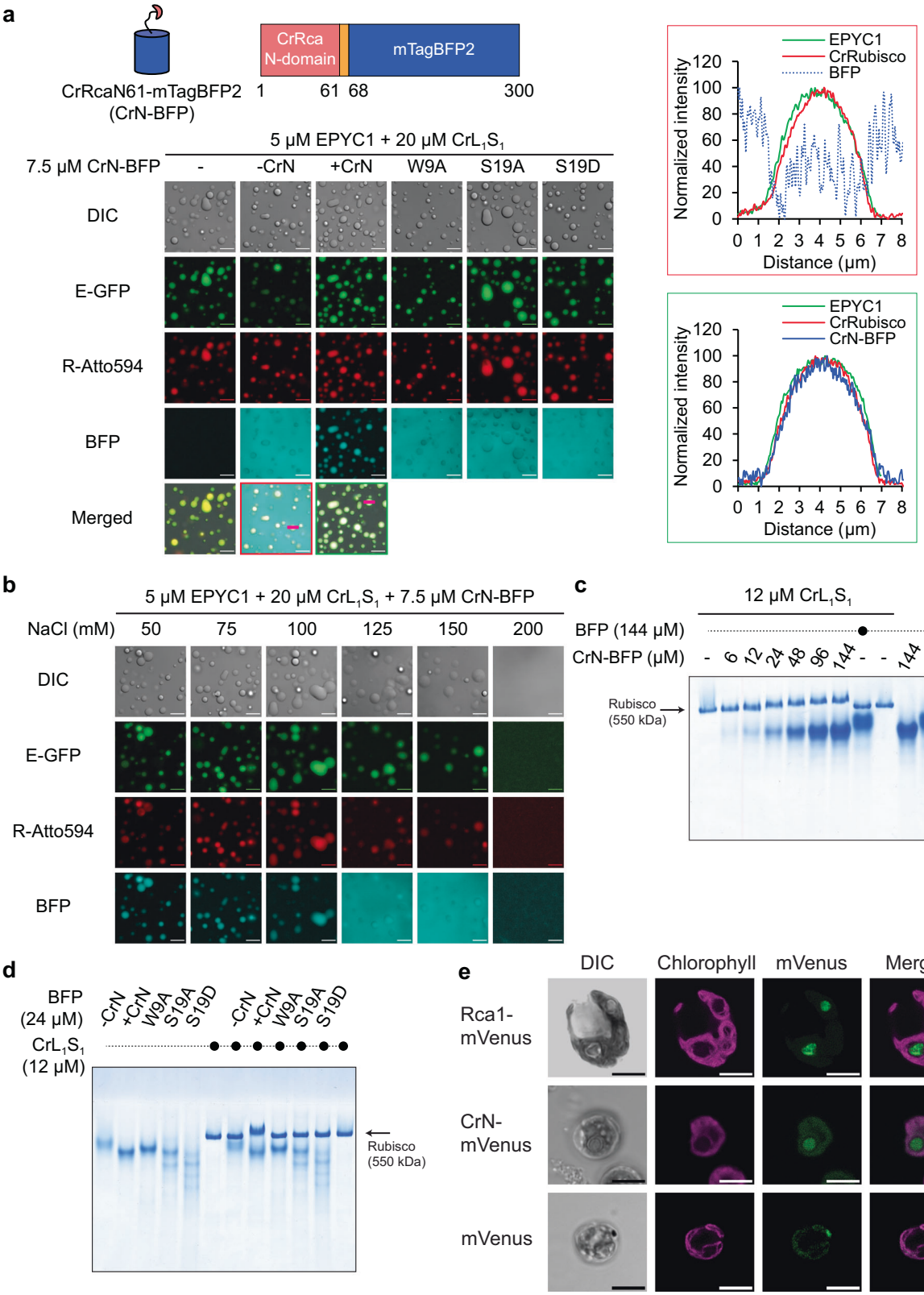

Methods

Strains and growth conditions

Amplification of plasmids constructed in this study was performed in E. coli DH5α (Thermo Fisher Scientific). Selected clones were cultivated in LB liquid media with the appropriate antibiotics at 37 °C and grown overnight. E. coli BL21 (DE3, Sigma-Aldrich) cells were used for recombinant production of the proteins used in this study.

Chlamydomonas reinhardtii strain CC-2677 (Chlamydomonas resource centre) was used to produce Rubisco in this study, cultured in Sueoka's high-salt medium under airlift conditions at ambient temperature.

C. reinhardtii strain CC-5168 was used for chloroplast transformation experiments[33]. CC-5168 were maintained on Tris-acetate phosphate (TAP) plates under dim light (5–10 μE/m²/s) at 23 °C.

Fig. 5 | The Rca N-terminal domain is sufficient to target a foreign protein to the Rubiscondensate. a Fusing the 61 residue N-terminal domain to mTagBFP2 enables partitioning to the EPYC1-Rubisco condensates. Functional point mutants abolish partitioning. Representative data of 2 independent experiments are shown ($n = 2$). **b** Partitioning is salt sensitive. Reactions contain 0.3 μM EPYC1-GFP and 0.2 μM Atto 594-labelled Rubisco. Scalebars, 10 μm. The experiment was performed once ($n = 1$). **c** The interaction causes a concentration-dependent gel shift of Rubisco as assessed by Native-PAGE. The experiment was performed four times independently, but using different protein concentrations ($n = 4$). **d** The gel shift is eliminated by amino acid substitutions. The experiment was performed once ($n = 1$). **e** CrN-mVenus localises to the pyrenoid, whereas mVenus alone is excluded in plastome edited *Chlamydomonas* strains. A strain expressing Rca-mVenus is used as a positive control. Micrographs were captured thrice for CrN-mVenus ($n = 3$), twice for mVenus untagged ($n = 2$) and once for Rca1-mVenus ($n = 1$). Scale bars: 5 μm. Source data are provided as a Source Data file.

Liquid cultures of CC-5168 were grown in conical flasks with TAP media with 100 μg/mL Spectinomycin at 23 °C, 120 rpm at 10 μE/m^2/s.

CC-5359 (expressing EPYC1-mVenus), CC-5357 (expressing RbcS1-mVenus) and CC-5358 (expressing Rca-mVenus)[8] were obtained from the Chlamydomonas resource centre.

Chloroplast transformation

Chloroplast transformation involved agitating an algal/DNA suspension with glass beads of 400–625 μm diameter[44]. CC-5168 was grown in a 400 mL TAP media with 100 μg/mL Spectinomycin, with the above-mentioned growth conditions, to early log phase (approx. 2×10^6 cells/ml). The culture was concentrated by centrifugation and resuspended in TAP media to a concentration of ~ 2×10^8 cells/mL (approx. 4 mL). 300 μL of cells were added to a sterilised 5 mL test tube containing 0.3 g of sterile glass beads. Circular plasmid DNA of 2.57 pmol (~ 10 – 12 μg) was added to the mixture and agitated vigorously at the maximum speed of a Vortex Genie II for 30 sec. 3.5 mL of 0.5% (w/v) molten agar (42 °C) was added to the tube and quickly poured onto HSM agar plates for selection of *psbH* rescue mutants. The plates were incubated at 23 °C in dim light (~ 2 μE/m^2/s) overnight, then transferred to a moderate light (~ 50 μE/m^2/s) the next day. Transformant colonies were picked after 2–3 weeks, and total genomic DNA was extracted from a small loopful of cells using the Chelex 100 method[45]. PCR amplification using a three-primer method[33] confirmed the integration of the foreign gene into the chloroplast genome.

Plasmids

Supplementary Data 1 shows the plasmids used in this study and the amino acid sequence of proteins produced and used. Supplementary Data 2 details the primers used.

pRSFDuet CrRca was generated by first amplifying the CrRca gene by PCR from *C. reinhardtii* CC-2677 cDNA and cloning it into the pGemT vector (Promega) (primers 1 and 2). Then, a follow-up PCR amplified CrRca with SacII and HindIII restriction sites for cloning into pHUE vector[46] (primers 3 and 4). A separate PCR reaction was used on the pRSFDuet vector encoding an unrelated gene to clone its backbone with EcoRI and HindIII restriction sites (primers 5 and 6). Thereafter, to generate pRSFDuet CrRca, PCR was utilised to amplify the CrRca gene along with its 5′ UTR elements while introducing EcoRI and HindIII restriction sites, the amplicon cloned into the pGemT vector (primers 7 and 8). Thereafter, restriction digestion using EcoRI and HindIII of this construct and the above prepared pRSFDuet backbone enabled the construction of pRSFDuet CrRca. Plasmids encoding CrRca N-domain mutations are all derived from pRSFDuet CrRca using primers as described in Supplementary Dataset 2.

pRSFDuet CrRca-mTagBFP2 (protein name shortened to CrRca-BFP in text) was also derived from pRSFDuet CrRca, where a PCR reaction was used to remove the stop codon and introduce BamHI and PstI restriction sites (primers 9 and 10). Then, the mTagBFP2 gene was amplified from pUC57 Kan mTagBFP2 using PCR, which also introduced BamHI and PstI restriction sites (primers 11 and 12) for insertion into pGemT. Restriction digestion using BamHI and PstI of these two plasmids enabled the assembly of pRSFDuet CrRca-mTagBFP2. This plasmid served as the template for further cloning to yield pRSFDuet mTagBFP2 (protein name shortened to BFP in text), pRSFDuet CrRcaN61-mTagBFP2 (protein name shortened to CrN-BFP in text) and its point mutants.

A codon optimised ORF (using codon usage optimiser, Saul Purton laboratory website, UCL) encoding residues 1–61 of CrRca fused to mVenus was synthesised by Genscript and inserted into pSRSapI[33] using SapI and SphI to give pSRSapI CrNmVenus to transform the *Chlamydomonas* chloroplast. pSRSapI mVenus was constructed in an analogous fashion.

Protein expression and purification

Protein purification was conducted using appropriate chromatography columns that are connected to an ÄKTA purifier system (Cytiva). Protein concentrations were calculated using extinction coefficients obtained using the ExPASy-ProtParam tool[47] from absorbance values at 280 nm as measured using a NanoDrop One (Thermo Fischer Scientific) instrument.

All mutants of CrRca used in this study (ΔN61, W9A, S19A, S19D) were expressed with an N-terminal His_6-Ub tag and were co-expressed with *E. coli* chaperonin-encoding pBADESL[48] in *E. coli* strain BL21 (DE3) cells. Cells were grown in LB media supplemented with 30 mg/L kanamycin (for selection of CrRca encoding plasmids and its variants) and 34 mg/L chloramphenicol for (for selection of pBADESL) at 37 °C with shaking at 200 rpm. Upon reaching the desired confluency, the culture was cooled and maintained at 23 °C for 1 hour before inducing chaperonin overexpression using 0.2% (w/v) L-arabinose. After 1 h, CrRca production was induced using 0.5 mM IPTG overnight. Cell lysis was conducted in Mg-ATP lysis buffer (50 mM Tris-HCl, pH 8, 50 mM NaCl, 10 mM imidazole, 10% (v/v) glycerol, 10 mM $MgCl_2$, 1 mM ATP) in the presence of 1 mM PMSF using ultrasonication after a lysozyme (0.3 mg lysozyme/mL of suspension) pretreatment on ice for 30 min. The soluble fraction was retained and loaded onto an IMAC column (HisTrap™ HP 5 mL, GE Healthcare) and washed using Mg-ATP HisTrap Buffer (20 mM Tris-HCl pH 8, 50 mM NaCl, 10 mM imidazole, 10% (v/v) glycerol, 10 mM $MgCl_2$, 1 mM ATP) with bound protein eluted using an imidazole gradient. The N-terminal His_6-ubiquitin moiety was cleaved[49] before subjecting CrRca to size-exclusion chromatography (Superdex 200 16/600, GE Healthcare) in 20 mM Tris-Cl, pH 8, 50 mM NaCl, and 10% (v/v) glycerol. Aliquots were then made of the pooled enriched CrRca, flash frozen and stored at − 80 °C. Prior to experiments, these aliquots were thawed and concentrated for use. All CrRca mutants were purified using the same protocol. All CrN-BFP variations were also purified using this protocol with the omission of 10 mM $MgCl_2$ and 1 mM ATP during cell lysis and IMAC.

pRSFDuet CrRca-mTagBFP2 (shortened to CrRca-BFP in text) was co-expressed with *Arabidopsis thaliana* chloroplast chaperonins as encoded by pAtC60αβ/C20[50], with induction solely by 0.5 mM IPTG for 18 hours at 23 °C. For its purification, an equal mass of cell pellets (CrRca-BFP co-expressed with pAtC60αβ/C20, and CrRca co-expressed with pBADESL) was mixed before lysis. The purification of CrRca-BFP then proceeds using the same protocol as utilised for the purification of CrRca and its mutants.

Rubisco activase from plants used in this study (OsRcaβ, AthRcaβ, AtRcaβ, and NtRca) were cloned into the pHUE vector and expressed in E. coli BL21 (DE3) cells before purification using IMAC, anion exchange, and size exclusion chromatography as described previously[23,28,51]. All

other Rubisco activases (RsCbbX, HnQO, and AfQ2O2) and mTagBFP2 were also purified in the same way[22–24].

EPYC1 was purified as described in Wunder, et al.[18] with the following deviation: after cleavage of the His_6-ubiquitin moiety, in place of dialysis, the material was subjected to a desalting column before the second exposure to IMAC. EPYC1-eGFP was purified through enrichment by IMAC without further processing[18]. Rubisco was purified from *C. reinhardtii* cells (CDC-2677) through ion-exchange chromatography and size-exclusion chromatography as described in Wunder, et al.[18].

Atto 594 labelling of Rubisco

Primary amines of Rubisco were labelled using Atto 594 NHS Ester (Atto 594 Protein Labelling Kit, Sigma-Aldrich, #68616) following the manufacturer's instructions. To polish the labelled protein, the labelled material was applied to an analytical size exclusion chromatography column (Superdex 200 increase 3.2/30 GL; Cytiva) that has been equilibrated with storage buffer (20 mM Tris-HCl, pH 8, 50 mM NaCl, 5% (v/v) Glycerol). Rubisco-containing fractions were concentrated, flash frozen and stored at −80 °C. When quantified according to the manufacturer's instructions, each CrRubisco holoenzyme was labelled with approximately two to three Atto 594 molecules.

Dylight 405 labelling of Activases

Primary amines of Activases were labelled using Dylight 405 NHS Ester (DyLight 405 Antibody Labeling kit, Thermo Scientific, #53020) following the manufacturer's instructions. To polish the labelled protein, the labelled material was applied to an analytical size exclusion chromatography column (Superdex 200 increase 3.2/30 GL; Cytiva) that has been equilibrated with storage buffer (20 mM Tris-HCl, pH 8, 50 mM NaCl, 5% (v/v) Glycerol). Activase-containing fractions were concentrated, flash frozen and stored at − 80 °C. When quantified according to the manufacturer's instructions, each activase complex was labelled with approximately two to eight Dylight 405 molecules.

Enzymatic assays

All assays were performed at 25 °C with a UV-1800 spectrophotometer and its associated UV probe v2.43 software (Shimadzu). ATPase activity of CrRca and its mutants was measured with 5 µM Rca protomer using a coupled enzymatic assay where ATP hydrolysis is coupled to the oxidation of NADH, monitored spectrophotometrically at 340 nm[23,27,51–53]. Rubisco activity and Rubisco activase activity assays were measured using a coupled enzyme spectrophotometric assay as previously described[23,53,54]. ECM holoenzyme was prepared by incubating CrRubisco apoenzyme (8 µM active sites) in 20 mM Tris-HCl, pH 8, 50 mM NaCl, 20 mM $MgCl_2$, and 20 mM $NaHCO_3$ at 25 °C for 15 minutes. RuBP-inhibited Rubisco (ER) was obtained by first incubating Rubisco apoenzyme (8 µM active sites) in 20 mM Tris-HCl, pH 8, 50 mM NaCl, and 4 mM EDTA at 25 °C for 10 min before the addition of 1 mM RuBP for a further incubation at 25 °C for another 15 min. Assay reactions were prepared to a final volume of 100 µL, and contained 100 mM Tricine-NaOH pH 8, 10 mM $MgCl_2$, 20 mM $NaHCO_3$, 1 mM DTT, 1 mM ATP, 1 mM RuBP, 0.2 mM NADH, 10 mM phosphocreatine, and coupling enzymes (including creatine phosphokinase for ATP-regeneration). The number of measurements reported refers to multiple measurements performed on the same sample.

Epifluorescence microscopy

Condensates and samples were prepared as 6 or 10 µL volume reactions, with 5 µL placed on a Nikon Inverted Ti microscope. Micrographs were recorded using the associated MetaMorph v7.8.10.0 software. Differential Interference Contrast (DIC) images were captured using DIC filter settings, GFP was detected using FITC filter settings, Atto 594 was detected initially using Cy5 filter settings (images in Fig. 1B) but subsequently detected using mCherry filter settings, and mTagBFP2 (BFP) and Dylight 405 was detected using DAPI filter settings. Image cropping, background subtraction, and merging were performed in Fiji[55].

Laser scanning confocal microscopy

Laser scanning confocal microscopy was conducted on an LSM 710 microscope (Zeiss) and its associated ZEN 2.3 (black) software. Samples were prepared to a final volume of 10 µL, with an incubation time of 1 min at 25 °C after EPYC1 addition. Imaging was performed with the following parameters: excitation laser of 488 nm at 2.5% intensity, pinhole set to 0.47 airy units. Laser power and master gain were adjusted such that the fluorescence intensity of 50 µM mEGFP was within the linear range of the detector. Images of mEGFP at each concentration were captured as 10 Z-stack slices at intervals of 0.26 µm. Three independent preparations of each mEGFP concentration was prepared, imaged, and averaged using the Fiji image processing software package to construct the standard curve. With these values, the graph for fluorescence intensity against mEGFP concentration was plotted and fitted as a linear function $y = ax + b$.

EPYC1-CrRubisco condensates were prepared as 10 µL samples in 20 mM Tris-HCl, pH 8, 50 mM NaCl, with 5 µL loaded for imaging. After allowing 1 min for condensates to settle, these samples were imaged as Z-stacks with each slice imaged at intervals of 0.26 µm, from below the glass slide till they fully cover the height of the condensates. Image acquisition was performed in the same way for three independent samples. Fiji imaging processing software was used to process these images. A region of interest was drawn on individual droplets, and the slice with maximum fluorescence intensity was retrieved and quantified using the multi-measure mode to estimate the C_{dense} of EPYC1. The C_{light} of EPYC1 was obtained by shifting the region of interest to the dilute phase, where its fluorescence intensity was selected from the last three slices in each sample.

The C_{dense} of Rubisco was estimated using an indirect approach. Sedimentation and densitometry data were used to calculate the mass of EPYC1 and Rubisco in pellet fractions. The C_{dense} of EPYC1 was then used to derive a volume fraction to the dense phase permitting a C_{dense} for Rubisco to be calculated.

Super-resolution laser-scanning microscopy (LSM)

All images of *Chlamydomonas* cells were recorded on a Zeiss LSM980 confocal microscope with Airyscan 2 module, using a 100 ×, 1.46 numerical aperture (NA) Plan-Apochromat oil-immersion lens (Carl Zeiss) operated with ZEN 3.4(blue) software. Microscopy samples were prepared by dropping a 10-13 µL culture volume on a 22 × 22 mm coverslip and overlaying another coverslip on top. For imaging, 639 nm for chlorophyll autofluorescence (2% laser power) and 488 nm for EGFP fluorescence (5% laser power) were used. Brightfield images were acquired at 488 nm using the T-PMT setting. Images were acquired at 2.5 × zoom to decrease acquisition time. The Airyscan detector (gain: 700 V) was used for image acquisition in frame mode with a final image size of 42.43 µm × 42.43 µm. Data analysis was performed with ZEN 3.3 (blue) software.

Fluorescence recovery after photobleaching (FRAP)

FRAP experiments conducted on condensates were conducted on a Nikon Inverted Ti2 confocal microscope equipped with a 1.46 NA x100 oil immersion lens at room temperature. Micrographs were recorded using the associated MetaMorph 7.10.4.407 software. Samples were prepared with a final volume of 10 µL with one labelled component at a time. The order of addition of proteins, which is consistent in all experiments performed was as follows: (1) CrRca (2) CrRubisco (3) EPYC1. After allowing 1 minute for condensates to settle, FRAP was conducted in the fluorescence channel of interest. Laser wavelength at 405 nm was used to image (75% power, 1000 ms exposure time) and bleach (70% power for 80 iterations) CrRca-

mTagBFP2. In samples formed with 7.5 µM CrRca, 5 µM EPYC1, and 20 µM CrRubisco, due to the difference in CrRca recruited into the condensates, bleaching was performed at 30% power for 80 iterations. Laser wavelength at 488 nm was used to image (20% power, 250 ms exposure time) and bleach (70% power for 50 iterations) EPYC1-mEGFP. Laser wavelength at 640 nm was used to image (100% power, 500 ms exposure time) and bleach (100% power for 80 iterations) Atto 594-labelled CrRubisco. Condensates were imaged for 2 seconds at 500 ms intervals prior to bleaching. After bleaching, images were captured every 1 s over 1 min to monitor for recovery of fluorescence intensity. Fiji v1.5.4 was used to process images. The number of bleaching events reported refers to different droplets bleached on 1–4 different samples.

Droplet sedimentation assays

Condensates were generated in 10 µL reactions for 2 min at room temperature (final buffer condition: 20 mM Tris-HCl, pH 8, and 50 mM NaCl) and dense and light phases were separated by centrifugation for 10 min at 21,100 × *g* at 20 °C. Following SDS-PAGE and Coomassie staining, the intensity of protein bands obtained in the pellet (droplet) and supernatant (bulk solution) was quantified using a number of methods. Gels in Supplementary Fig. S1 were scanned using a GS-800TM Calibrated Densitometer (Bio Rad) and analysed using Quantity One v4.6.8 (Bio-Rad). Two sets of data for Fig. 4C were imaged using a ChemiDoc system (Bio-Rad) and analysed on ImageLab 6.1 (Bio-Rad), and one set was generated using a desk scanner and analysed using Fiji v.1.54 f. Using Quantity One and ImageLab, lanes to be quantified were manually framed for semi-automatic detection of protein bands. Background subtraction was performed via the lane-based rolling disk setting. The band volumes (average OD of the band times its area, INT x mm^2) of the protein of interest were then determined. The proportion of a given protein sedimented in the experiment was obtained by dividing the volume of the protein in the pellet fraction with the sum of the volumes of the protein in the supernatant and pellet fraction. For CrRubisco, the Rubisco large subunit band was quantified.

Reporting summary

Further information on research design is available in the Nature Portfolio Reporting Summary linked to this article.

Data availability

The data acquired and analysed during this study are available at the NTU Research Data Repository under https://doi.org/10.21979/N9/EYYRYQ [https://doi.org/10.21979/N9/EYYRYQ]. Unless otherwise stated, all data supporting the results of this study can be found in the article, supplementary, and source data files. Source data are provided in this paper.

References

1. Prywes, N., Phillips, N. R., Tuck, O. T., Valentin-Alvarado, L. E. & Savage, D. F. Rubisco function, evolution, and engineering. *Annu. Rev. Biochem.* **92**, 385–410 (2023).
2. Parry, M. A. J., Keys, A. J., Madgwick, P. J., Carmo-Silva, A. E. & Andralojc, P. J. Rubisco regulation: a role for inhibitors. *J. Exp. Bot.* **59**, 1569–1580 (2008).
3. Mueller-Cajar, O. et al. The diverse AAA+ machines that repair inhibited Rubisco active sites. *Front. Mol. Biosci.* **4**, https://doi.org/10.3389/fmolb.2017.00031 (2017).
4. Rae, B. D., Long, B. M., Badger, M. R. & Price, G. D. Functions, compositions, and evolution of the two types of carboxysomes: polyhedral microcompartments that facilitate CO2 fixation in cyanobacteria and some proteobacteria. *Microbiol. Mol. Biol. Rev.* **77**, 357–379 (2013).
5. Hennacy, J. H. & Jonikas, M. C. Prospects for engineering biophysical CO2 concentrating mechanisms into land plants to enhance yields. *Annu. Rev. Plant Biol.* **71**, 461–485 (2020).
6. He, S., Crans, V. L. & Jonikas, M. C. The pyrenoid: the eukaryotic CO2-concentrating organelle. *Plant Cell* **35**, 3236–3259 (2023).
7. Wunder, T., Oh, Z. G. & Mueller-Cajar, O. C. O. 2) -fixing liquid droplets: Towards a dissection of the microalgal pyrenoid. *Traffic* **20**, 380–389 (2019).
8. Mackinder, L. C. et al. A repeat protein links Rubisco to form the eukaryotic carbon-concentrating organelle. *Proc. Natl. Acad. Sci. USA* **113**, 5958–5963 (2016).
9. He, S. et al. The structural basis of Rubisco phase separation in the pyrenoid. *Nat. Plants* **6**, 1480–1490 (2020).
10. Ang, W. S. L., How, J. A., How, J. B. & Mueller-Cajar, O. The stickers and spacers of Rubiscondensation: assembling the centrepiece of biophysical CO2-concentrating mechanisms. *J. Exp. Bot.* **74**, 612–626 (2023).
11. Lau, C. S., Dowle, A., Thomas, G. H., Girr, P. & Mackinder, L. C. M. A phase-separated CO2-fixing pyrenoid proteome determined by TurboID in Chlamydomonas reinhardtii. *Plant Cell* **35**, 3260–3279 (2023).
12. Mackinder, L. C. M. et al. A spatial interactome reveals the protein organization of the algal CO2-concentrating mechanism. *Cell* **171**, 133–147 (2017).
13. Wang, L. et al. A chloroplast protein atlas reveals punctate structures and spatial organization of biosynthetic pathways. *Cell* **186**, 3499–3518 (2023).
14. Holehouse, A. S. & Alberti, S. Molecular determinants of condensate composition. *Mol. Cell* **85**, 290–308 (2025).
15. Freeman Rosenzweig, E. S. et al. The eukaryotic CO2-concentrating organelle is liquid-like and exhibits dynamic reorganization. *Cell* **171**, 148–162 (2017).
16. Pollock, S. V., Colombo, S. L., Prout, D. L. Jr., Godfrey, A. C. & Moroney, J. V. Rubisco activase is required for optimal photosynthesis in the green alga Chlamydomonas reinhardtii in a low-CO2 atmosphere. *Plant Physiol.* **133**, 1854–1861 (2003).
17. Meyer, M. T. et al. Assembly of the algal CO(2)-fixing organelle, the pyrenoid, is guided by a Rubisco-binding motif. *Sci. Adv.* **6**, https://doi.org/10.1126/sciadv.abd2408 (2020).
18. Wunder, T., Cheng, S. L. H., Lai, S. K., Li, H. Y. & Mueller-Cajar, O. The phase separation underlying the pyrenoid-based microalgal Rubisco supercharger. *Nat. Commun.* **9**, 5076 (2018).
19. Portis, A. R., Li, C. S., Wang, D. F. & Salvucci, M. E. Regulation of Rubisco activase and its interaction with Rubisco. *J. Exp. Bot.* **59**, 1597–1604 (2008).
20. Wang, Z.-Y., Snyder, G. W., Esau, B. D., Portis, A. R. Jr & Ogren, W. L. Species-dependent variation in the interaction of substrate-bound ribulose-1,5-bisphosphate carboxylase/oxygenase (Rubisco) and Rubisco activase. *Plant Physiol.* **100**, 1858–1862 (1992).
21. Flecken, M. et al. Dual functions of a Rubisco activase in metabolic repair and recruitment to carboxysomes. *Cell* **183**, 457–473 (2020).
22. Mueller-Cajar, O. et al. Structure and function of the AAA+ protein CbbX, a red-type Rubisco activase. *Nature* **479**, 194–199 (2011).
23. Tsai, Y. C., Lapina, M. C., Bhushan, S. & Mueller-Cajar, O. Identification and characterization of multiple rubisco activases in chemoautotrophic bacteria. *Nat. Commun.* **6**, 8883 (2015).
24. Tsai, Y. C., Liew, L., Guo, Z., Liu, D. & Mueller-Cajar, O. The CbbQO-type rubisco activases encoded in carboxysome gene clusters can activate carboxysomal form IA rubiscos. *J. Biol. Chem.* **298**, 101476 (2022).
25. Esau, B. D., Snyder, G. W. & Portis, A. R. Differential effects of N- and C-terminal deletions on the two activities of rubisco activase. *Arch. Biochem. Biophys.* **326**, 100–105 (1996).

26. van de Loo, F. J. & Salvucci, M. E. Activation of ribulose-1,5-bisphosphate carboxylase/oxygenase (Rubisco) involves Rubisco activase Trp16. *Biochemistry* **35**, 8143–8148 (1996).
27. Stotz, M. et al. Structure of green-type Rubisco activase from tobacco. *Nat. Struct. Mol. Biol.* **18**, 1366–U1378 (2011).
28. Shivhare, D., Ng, J., Tsai, Y. C. & Mueller-Cajar, O. Probing the rice Rubisco-Rubisco activase interaction via subunit hetero-oligomerization. *Proc. Natl. Acad. Sci. USA* **116**, 24041–24048 (2019).
29. Lemeille, S., Turkina, M. V., Vener, A. V. & Rochaix, J. D. Stt7-dependent phosphorylation during state transitions in the green alga Chlamydomonas reinhardtii. *Mol. Cell Proteom.* **9**, 1281–1295 (2010).
30. Wang, H. et al. The global phosphoproteome of Chlamydomonas reinhardtii reveals complex organellar phosphorylation in the flagella and thylakoid membrane. *Mol. Cell Proteom.* **13**, 2337–2353 (2014).
31. Baginsky, S. Protein phosphorylation in chloroplasts - a survey of phosphorylation targets. *J. Exp. Bot.* **67**, 3873–3882 (2016).
32. Boex-Fontvieille, E. et al. Phosphorylation pattern of Rubisco activase in Arabidopsis leaves. *Plant Biol.* **16**, 550–557 (2014).
33. Wannathong, T., Waterhouse, J. C., Young, R. E., Economou, C. K. & Purton, S. New tools for chloroplast genetic engineering allow the synthesis of human growth hormone in the green alga Chlamydomonas reinhardtii. *Appl. Microbiol. Biotechnol.* **100**, 5467–5477 (2016).
34. Kim, S. Y. et al. In vivo evidence for a regulatory role of phosphorylation of Arabidopsis Rubisco activase at the Thr78 site. *Proc. Natl. Acad. Sci. USA* **116**, 18723–18731 (2019).
35. Boeynaems, S. et al. Poly(A)-binding protein is an ataxin-2 chaperone that regulates biomolecular condensates. *Mol. Cell* **83**, 2020–2034 (2023).
36. Liboy-Lugo, J. M. et al. G3BP isoforms differentially affect stress granule assembly and gene expression during cellular stress. *Mol. Biol. Cell* **35**, ar140 (2024).
37. Kunz, H. H., Armbruster, U., Muhlbauer, S., de Vries, J. & Davis, G. A. Chloroplast ion homeostasis - what do we know and where should we go? *N. Phytol.* **243**, 543–559 (2024).
38. Malhotra, B. & Glass, A. Potassium Fluxes in Chlamydomonas reinhardtii (II. Compartmental Analysis). *Plant Physiol.* **108**, 1537–1545 (1995).
39. Robinson, S. P. & Downton, W. J. Potassium, sodium, and chloride content of isolated intact chloroplasts in relation to ionic compartmentation in leaves. *Arch. Biochem. Biophys.* **228**, 197–206 (1984).
40. Yamagishi, A., Satoh, K. & Katoh, S. The concentrations and thermodynamic activities of cations in intact Bryopsis chloroplasts. *Biochim. Biophys. Acta Bioenerg.* **637**, 252–263 (1981).
41. Holehouse, A. S. & Kragelund, B. B. The molecular basis for cellular function of intrinsically disordered protein regions. *Nat. Rev. Mol. Cell Biol.* **25**, 187–211 (2024).
42. Atkinson, N., Mao, Y., Chan, K. X. & McCormick, A. J. Condensation of Rubisco into a proto-pyrenoid in higher plant chloroplasts. *Nat. Commun.* **11**, 6303 (2020).
43. Atkinson, N., Stringer, R., Mitchell, S. R., Seung, D. & McCormick, A. J. SAGA1 and SAGA2 promote starch formation around proto-pyrenoids in Arabidopsis chloroplasts. *Proc. Natl. Acad. Sci. USA* **121**, e2311013121 (2024).
44. Kindle, K. L., Richards, K. L. & Stern, D. B. Engineering the chloroplast genome: techniques and capabilities for chloroplast transformation in Chlamydomonas reinhardtii. *Proc. Natl. Acad. Sci. USA* **88**, 1721–1725 (1991).
45. Werner, R. & Mergenhagen, D. Mating type determination of Chlamydomonas reinhardtii by PCR. *Plant Mol. Biol. Report.* **16**, 295–299 (1998).
46. Catanzariti, A.-M., Soboleva, T. A., Jans, D. A., Board, P. G. & Baker, R. T. An efficient system for high-level expression and easy purification of authentic recombinant proteins. *Protein Sci.* **13**, 1331–1339 (2004).
47. Gasteiger, E. et al. *The Proteomics Protocols Handbook* (Humana Press, 2005).
48. Ewalt, K. L., Hendrick, J. P., Houry, W. A. & Hartl, F. U. In vivo observation of polypeptide flux through the bacterial chaperonin system. *Cell* **90**, 491–500 (1997).
49. Baker, R. T. et al. Using deubiquitylating enzymes as research tools. *Methods Enzymol.* **398**, 540–554 (2005).
50. Aigner, H. et al. Plant RuBisCo assembly in E. coli with five chloroplast chaperones including BSD2. *Science* **358**, 1272–1278 (2017).
51. Shivhare, D. & Mueller-Cajar, O. In vitro characterization of thermostable CAM Rubisco activase reveals a Rubisco interacting surface loop. *Plant Physiol.* **174**, 1505–1516 (2017).
52. Kreuzer, K. N. & Jongeneel, C. V. Escherichia coli phage T4 topoisomerase. *Methods Enzymol.* **100**, 144–160 (1983).
53. Loganathan, N., Tsai, Y. C. & Mueller-Cajar, O. Characterization of the heterooligomeric red-type rubisco activase from red algae. *Proc. Natl. Acad. Sci. USA* **113**, 14019–14024 (2016).
54. Lan, Y. & Mott, K. A. Determination of apparent K(m) values for Ribulose 1,5-bisphosphate carboxylase/oxygenase (Rubisco) activase using the spectrophotometric assay of Rubisco activity. *Plant Physiol.* **95**, 604–609 (1991).
55. Schindelin, J. et al. Fiji: an open-source platform for biological-image analysis. *Nat. Methods* **9**, 676–682 (2012).

Acknowledgements

The research was supported by Ministry of Education of Singapore grants MOE2019-T3-1-012 (O.M.-C.), Tier 1 grant RG36/23 (O.M.-C.) and the National Research Foundation of Singapore (NRF-NRFI07-2021-0004) (O. M.-C.).

Author contributions

J.B.H. designed and performed most biochemical experiments. C.W.P. conducted the experiments during manuscript revision. Y.S.N. performed in vivo *Chlamydomonas* work. T.W. contributed to exploratory experiments. O.M.-C. supervised the work and wrote the paper with J.B.H.

Competing interests

The authors declare no competing interests.

Additional information

Supplementary information The online version contains supplementary material available at https://doi.org/10.1038/s41467-026-70724-5.

Correspondence and requests for materials should be addressed to Oliver Mueller-Cajar.

Peer review information *Nature Communications* thanks the anonymous reviewers for their contribution to the peer review of this work. A peer review file is available.

Reprints and permissions information is available at http://www.nature.com/reprints

Publisher's note Springer Nature remains neutral with regard to jurisdictional claims in published maps and institutional affiliations.

Open Access This article is licensed under a Creative Commons Attribution-NonCommercial-NoDerivatives 4.0 International License, which permits any non-commercial use, sharing, distribution and reproduction in any medium or format, as long as you give appropriate credit to the original author(s) and the source, provide a link to the Creative Commons licence, and indicate if you modified the licensed material. You do not have permission under this licence to share adapted material derived from this article or parts of it. The images or other third party material in this article are included in the article's Creative Commons licence, unless indicated otherwise in a credit line to the material. If material is not included in the article's Creative Commons licence and your intended use is not permitted by statutory regulation or exceeds the permitted use, you will need to obtain permission directly from the copyright holder. To view a copy of this licence, visit http://creativecommons.org/licenses/by-nc-nd/4.0/.

© The Author(s) 2026